Chapter 11

Electro-magnetohydrodynamic Casson nanomaterial flow over a nonlinearly stretched surface *

11.1 Introduction

Casson fluid, proposed by Casson in 1959, is a shear thinning fluid that assumes infinite viscosity at zero shear-rate, and vice versa. Human blood, honey, tomato sauce, jelly, and concentrated fruit juices are a few examples that follow the Casson nanofluid model. Different nanoparticle shape and radius exhibit different thermal properties that are beneficial in industrial and biomedical fields. The relative movement of the fluid with the boundary is characterized with the aid of slip constraint. For its biomedical applicability, the dynamics of electro-magnetohydrodynamic flow of blood-gold nanomaterial over a nonlinearly stretching surface utilizing the Casson model has been elucidated numerically. The impact of second-order hydrodynamic-slip, nanoparticle radius, first-order thermal-slip, inter-particle spacing and non-uniform heat source are also accounted. The modeled flow equations are transmuted into a nonlinear system of first-order ODEs (with the aid of apposite similarity variables) which are then resolved numerically utilizing the finite-difference based *bvp*5*c* scheme. The current chapter finds its application in radiofrequency ablation, magnetic resonance imaging, cancer therapy, and targeted drug delivery. This numerical exploration makes an attempt in answering the following research questions:

- How does the administration of external electric-field affect the flow?

*Communicated in: Numerical Heat Transfer, Part B: Fundamentals (Taylor & Francis).

- What impact does the addition of gold nanoparticles with varying radius and inter-particle spacing have on Casson nanofluid flow?
- How does second-order hydrodynamic-slip constraint affect the flow?
- What effect does non-uniform heat source have on the thermal field?
- How does the physical quantities sequel to the changes in key parameters?

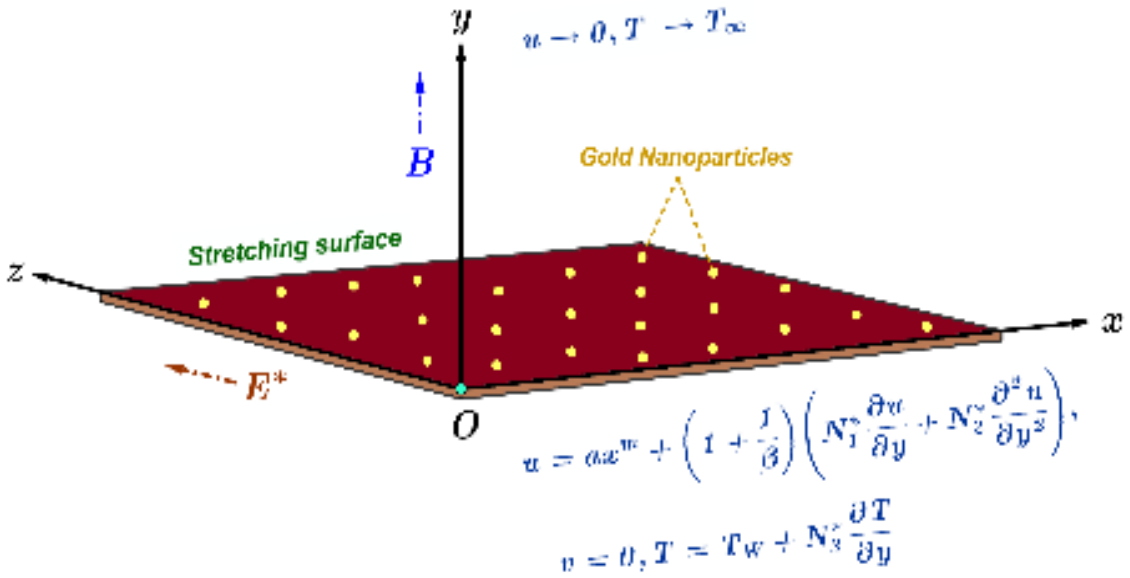

Figure 11.1: Geometrical Frame

11.2 Mathematical Frame

The two-dimensional steady electro-magnetohydrodynamic flow of blood-gold nanomaterial over a nonlinearly stretching surface (with velocity $u_w = ax^m$) utilizing the Casson model is considered. A magnetic-field of intensity $B = B_0\, x^{\frac{m-1}{2}}$ and an electric-field of intensity $E^* = E_0\, x^{\frac{m-1}{2}}$ are administered externally normal to the fluid flow (see Daniel et al., 2018). The impact of 2nd order hydrodynamic-slip, gold nanoparticles of different inter-particle spacing and radius, first order thermal-slip and non-uniform heat source (NHS) are also accounted. The geometrical scheme of the flow has been shown in Figure 11.1.

The governing equations modelled using the above assumptions are given by (see J. Raza, Farooq, Mebarek-Oudina, & Mahanthesh, 2019; Zhou et al., 2021; Fang & Aziz, 2010):

$$\frac{\partial u}{\partial x}+\frac{\partial v}{\partial y}=0 \tag{11.2.1}$$

$$u\frac{\partial u}{\partial x}+v\frac{\partial u}{\partial y}=\frac{\mu_{nf}}{\rho_{nf}}\left(1+\frac{1}{\beta}\right)\frac{\partial^2 u}{\partial y^2}+\frac{\sigma_{nf}}{\rho_{nf}}\left(E^*B-B^2u\right) \tag{11.2.2}$$

$$u\frac{\partial T}{\partial x}+v\frac{\partial T}{\partial y}=\frac{k_{nf}}{(\rho C_p)_{nf}}\frac{\partial^2 T}{\partial y^2}+\frac{q'''}{(\rho C_p)_{nf}} \tag{11.2.3}$$

subject to the boundary conditions (see Abdelmalek et al., 2020; J. Raza et al., 2019):

$$At\ y=0\ :\ u=ax^m+\left(1+\frac{1}{\beta}\right)\left(N_1^*\frac{\partial u}{\partial y}+N_2^*\frac{\partial^2 u}{\partial y^2}\right)\ ,\ v=0\ ,\ T=T_w+N_3^*\frac{\partial T}{\partial y}$$

$$As\ y\to\infty\ :\ u\to 0,\ T\to T_\infty$$

where $q'''=\frac{k_{nf}}{x\ \vartheta_{nf}}\left\{A^*\left(T_w-T_\infty\right)u+B^*\left(T-T_\infty\right)u_w\right\}$ with $A^*>0,\ B^*>0$ is the non-uniform heat source, $N_1^*\,(>0)=N_1x^{\frac{1-m}{2}}$ is the first order velocity-slip factor, $N_2^*\,(<0)=N_2\ x^{1-m}$ is the second order velocity-slip factor, and $N_3^*\,(>0)=N_3\ x^{\frac{1-m}{2}}$ is the first order thermal-slip factor.

Consider the following similarity transformations (see Mabood et al., 2015; Basir et al., 2021):

$$u=ax^m f'(\eta)\,,\ v=-\sqrt{\frac{a\vartheta_f\,(m+1)}{2}}\ x^{\frac{m-1}{2}}\left(f(\eta)+\left(\frac{m-1}{m+1}\right)\eta\ f'(\eta)\right),$$

$$\eta=\sqrt{\frac{a\,(m+1)}{2\vartheta_f}}\ yx^{\frac{m-1}{2}},\ \theta(\eta)=\frac{T-T_\infty}{T_w-T_\infty}$$

Using the above defined similarity transformations, Equations (11.2.1) – (11.2.3) are converted into:

$$f\,''' = \frac{1}{1+\frac{1}{\beta}}\left\{\frac{A_2}{A_1}\left(\frac{2m}{m+1}\,(f\,')^2 - f f\,''\right) - \frac{A_3}{A_1}\left(\frac{2}{m+1}\right)M\,(E - f\,')\right\} \tag{11.2.4}$$

$$\theta\,'' = -\left\{\frac{A_5}{A_4}\,Pr\;f\;\theta\,' + \frac{A_2}{A_1}\left(\frac{2}{m+1}\right)(A^*\;f\,' + B^*\;\theta)\right\} \tag{11.2.5}$$

subject to the boundary conditions

$$f\,(0) = 0,\;\; f\,'(0) = 1 + \left(1 + \frac{1}{\beta}\right)\left(\sqrt{\frac{m+1}{2}}\;L_1\;f\,''(0) + \left(\frac{m+1}{2}\right)L_2\;f\,'''(0)\right),$$

$$\theta\,(0) = 1 + \sqrt{\frac{m+1}{2}}\;L_3\;\theta\,'(0)\,,\;\; f\,'(\infty) \to 0,\;\; \theta\,(\infty) \to 0.$$

where the dimensionless parameters are given in appendix I.

The nanofluid models incorporated are (see Sun et al., 2022):

$$\text{Effective Dynamic Viscosity} \;\; : \;\; \frac{\mu_{nf}}{\mu_f} = 1 + 2.5\;\phi + 4.5\left\{\frac{1}{\left(\frac{h}{R_{np}}\right)\left(2 + \frac{h}{R_{np}}\right)\left(1 + \frac{h}{R_{np}}\right)^2}\right\} = A_1$$

$$\text{Effective Density} \;\; : \;\; \frac{\rho_{nf}}{\rho_f} = (1-\phi) + \phi\left(\frac{\rho_{np}}{\rho_f}\right) = A_2$$

$$\text{Effective Electrical Conductivity} \;\; : \;\; \frac{\sigma_{nf}}{\sigma_f} = 1 + \frac{3\left(\frac{\sigma_{np}}{\sigma_f} - 1\right)\phi}{\left(\frac{\sigma_{np}}{\sigma_f} + 2\right) - \left(\frac{\sigma_{np}}{\sigma_f} - 1\right)\phi} = A_3$$

$$\text{Effective Thermal Conductivity} \;\; : \;\; \frac{k_{nf}}{k_f} = \frac{k_{np} + 2k_f - 2\phi\,(k_f - k_{np})}{k_{np} + 2k_f + \phi\,(k_f - k_{np})} = A_4$$

$$\text{Effective Specific Heat} \;\; : \;\; \frac{(\rho C_P)_{nf}}{(\rho C_P)_f} = (1-\phi) + \phi\left(\frac{(\rho C_p)_{np}}{(\rho C_p)_f}\right) = A_5$$

The physical quantities are given by (see Daniel et al., 2018; J. Raza et al., 2019; Zhou et al., 2021):

$$\text{Local drag coefficient} \quad : \quad Cf_x = \frac{\tau_\omega}{\rho_f \ (u_w)^2} = \frac{\mu_{nf}}{\rho_f \ (u_w)^2} \ \left(1 + \frac{1}{\beta}\right) \ \left.\frac{\partial u}{\partial y}\right|_{y=0}$$

$$\Rightarrow \ Cf_x \ Re_x^{1/2} = A_1 \ \sqrt{\frac{m+1}{2}} \left(1 + \frac{1}{\beta}\right) f \ ''(0)$$

$$\text{Local Nusselt number} \quad : \quad Nu_x = \frac{x \ q_\omega}{k_f \ (T_w - T_\infty)} = \frac{-\ x \ k_{nf}}{k_f \ (T_w - T_\infty)} \ \left.\frac{\partial T}{\partial y}\right|_{y=0}$$

$$\Rightarrow \ Nu_x \ Re_x^{-1/2} = -A_4 \ \sqrt{\frac{m+1}{2}} \ \theta \ '(0).$$

where $Re_x = \frac{x u_w}{\vartheta_f}$ is the local Reynold's number.

11.3 Numerical Frame & Validation

The nonlinear ordinary differential equations given in Equations (11.2.4) − (11.2.5) are reduced to a system of first order ODEs by setting:

$$\Gamma_1 = f, \ \Gamma_2 = f \ ', \ \Gamma_3 = f \ '', \ \Gamma_4 = \theta, \ \Gamma_5 = \theta \ '$$

The reduced system of the first-order ODE is given by:

$\Gamma_1^{'} = \Gamma_2, \ \Gamma_2^{'} = \Gamma_3,$

$\Gamma_3^{'} = \frac{1}{\left(1+\frac{1}{\beta}\right)} \left\{ \left(\frac{A_2}{A_1}\right) \left(\frac{2m}{m+1}\right) (\Gamma_2)^2 - \left(\frac{A_2}{A_1}\right) \Gamma_1 \ \Gamma_3 - \left(\frac{A_3}{A_1}\right) \left(\frac{2}{m+1}\right) M \ (E - \Gamma_2) \right\},$

$\Gamma_4^{'} = \Gamma_5,$

$\Gamma_5^{'} = -\left\{ \left(\frac{A_5 \ Pr}{A_4}\right) \Gamma_1 \ \Gamma_5 + \left(\frac{A_2}{A_1}\right) \left(\frac{2}{m+1}\right) (A^* \ \Gamma_2 + B^* \ \Gamma_4) \right\}.$

with

$$\Gamma_1 (0) = 0, \ \Gamma_2 (0) = 1 + \left(1 + \tfrac{1}{\beta}\right) \left(\sqrt{\tfrac{m+1}{2}} \ L_1 \ \Gamma_3 (0) + \left(\tfrac{m+1}{2}\right) L_2 \ \Gamma_3^{'} (0) \right),$$

$$\Gamma_4 (0) = 1 + \sqrt{\tfrac{m+1}{2}} \ L_3 \ \Gamma_5 (0), \ \Gamma_2 (\infty) \to 0, \ \Gamma_4 (\infty) \to 0.$$

Table 11.1: Resemblance of $-\theta'(0)$ for ordinary fluid when $Pr_f = 1$

n	$-\theta'(\mathbf{0})$		
	Rana & Bhargava, 2012	**Mabood et al., 2015**	**Present Study**
0.2	0.6113	0.61131	0.6113101754
0.5	0.5967	0.59668	0.5966869638
1.5	0.5768	0.57686	0.5768695043
2	-	0.57245	0.5724552833
3	0.5672	0.56719	0.5671905106
4	-	0.56415	0.5641562432
10	0.5578	0.55783	0.5578319176

Table 11.2: Thermophysical properties of blood and gold

Property	**Blood (base fluid)**	**Gold (nanoparticle)**
$\boldsymbol{\rho}$	1050	19300
$\boldsymbol{C_p}$	3617	129
$\boldsymbol{k}$	0.52	318
$\boldsymbol{\sigma}$	1090	$4.1 * 10^6$

The boundary constraints at infinity are dimensioned to 4 since there is no substantial difference in the numerical outcomes on using higher values of the similarity variable, and the flow fields follow the boundary constraints asymptotically. $Pr = 21$, $\phi = 0.02$, $m = 2$, $M = A^* = B^* = L_1 = L_3 = 0.5$, $E = 0.05$, $\beta = 5$, $L_2 = -0.5$, and $h = R_{np} = 1$ have been chosen as the default values. The above system of 1st order ODEs is solved numerically with the aid of *bvp*5*c* scheme in MATLAB with an absolute error tolerance of 10^{-8}. The accuracy of the numerical scheme has been validated through a restrictive analysis with the previously published works of (Rana & Bhargava, 2012) and (Mabood et al., 2015) [see Table 11.1] and a notable covenant is noted.

11.4 Results & Discussion

The impact of pertinent parameters on the velocity profile ($f'(\eta)$) and the temperature profile ($\theta(\eta)$) has been illustrated through Figures 11.2 - 11.16. The thermophysical properties of blood and gold nanoparticle are mentioned in Table 11.2.

The reduction in $f'(\eta)$ with respect to the augmenting values of m has been depicted in Figure 11.2. The introduction of M activates the generation of Lorentz force that reduces $f'(\eta)$ (see Figure 11.3). A reverse nature is observed for $f'(\eta)$ with the introduction of E (see Figure 11.4). Figure 11.5 elucidates the negative impact of β on the nanofluid velocity. The addition of gold-nanoparticles increases the fluid's viscosity and thereby reduces $f'(\eta)$ (see Figure 11.6). The negative impact of inter-particle spacing of gold-nanoparticles on $f'(\eta)$ has been illustrated via Figure 11.7. An increase in the radius of gold-nanoparticles reduces the nanofluid viscosity and thereby augments $f'(\eta)$ (see Figure 11.8). The destructive effect of 1st order velocity-slip parameter and the constructive effect of 2nd order velocity-slip parameter on $f'(\eta)$ have been depicted using Figure 11.9 and Figure 11.10, respectively.

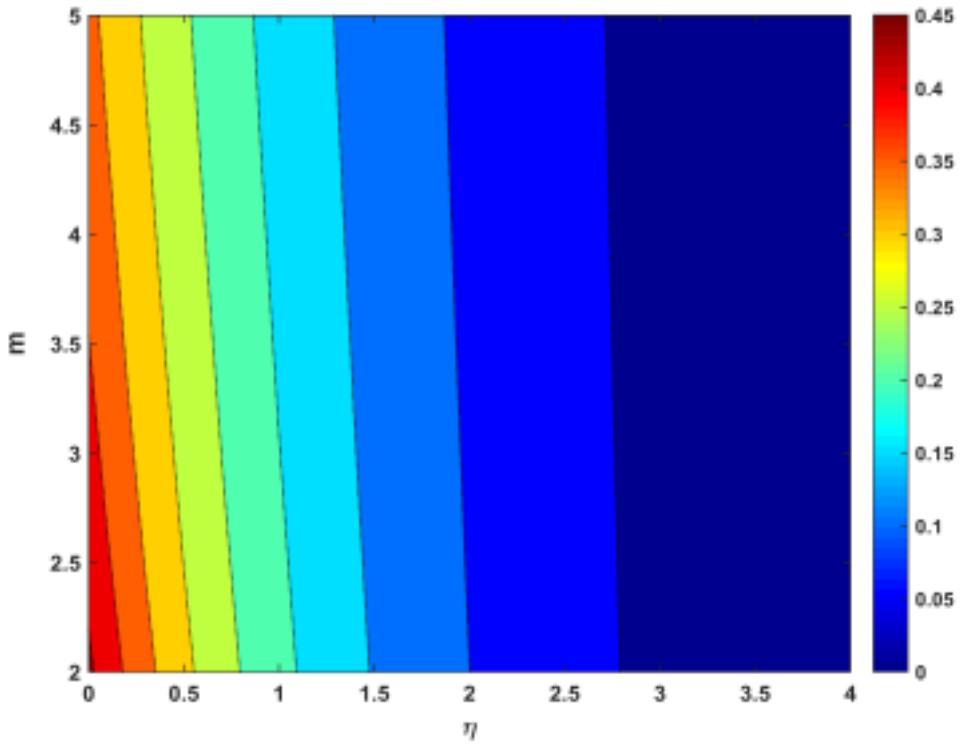

Figure 11.2: Deviations in $f'(\eta)$ with m

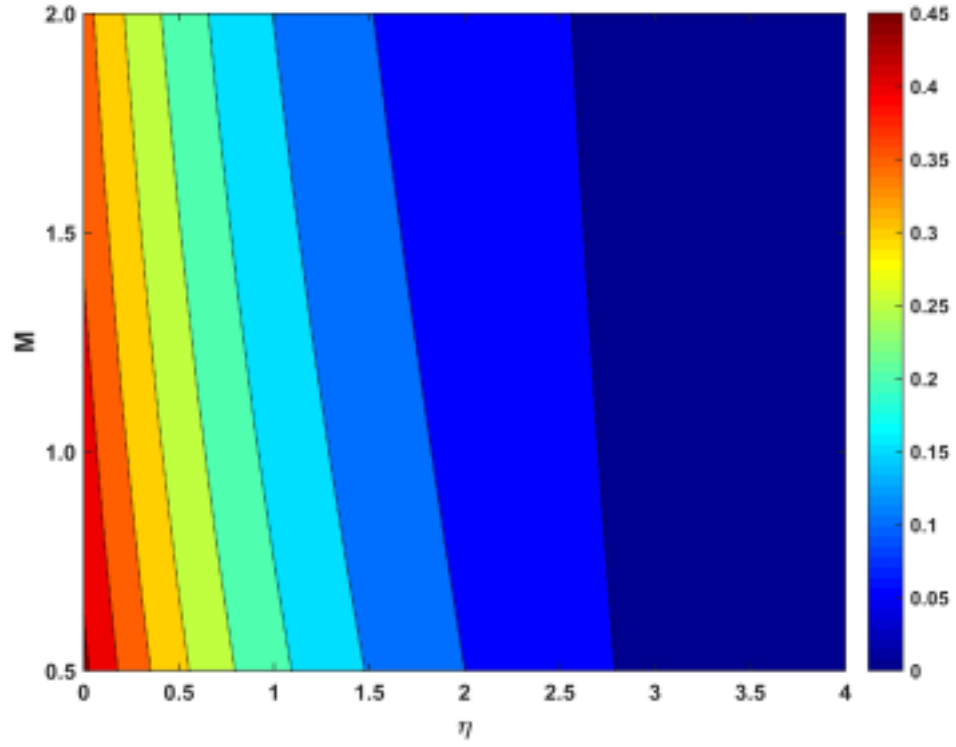

Figure 11.3: Deviations in $f'(\eta)$ with M

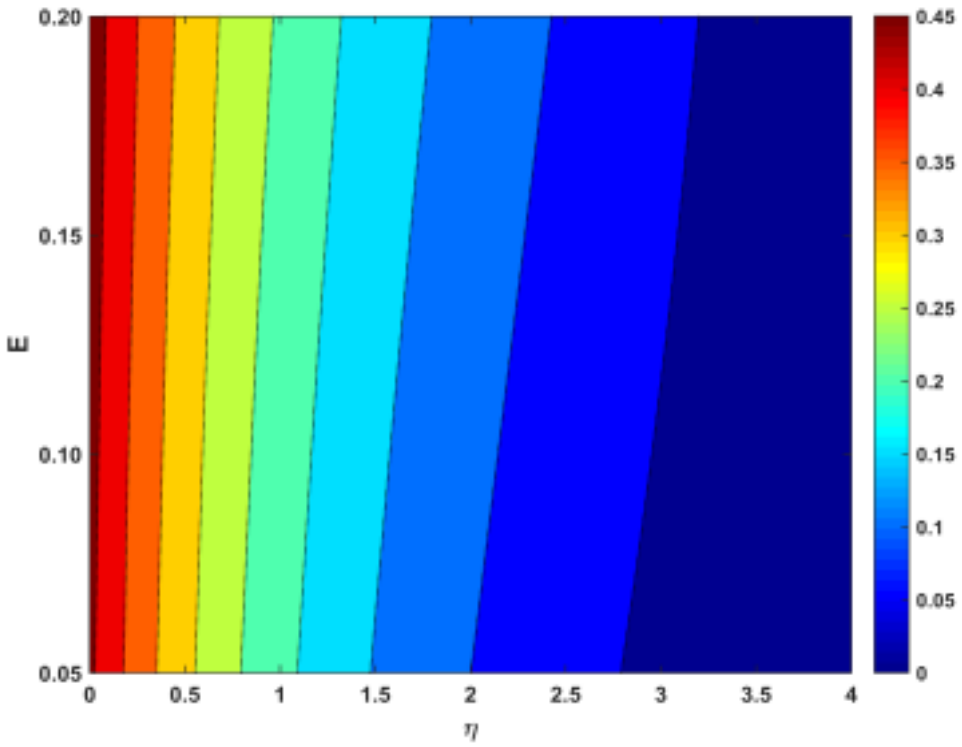

Figure 11.4: Deviations in $f'(\eta)$ with E

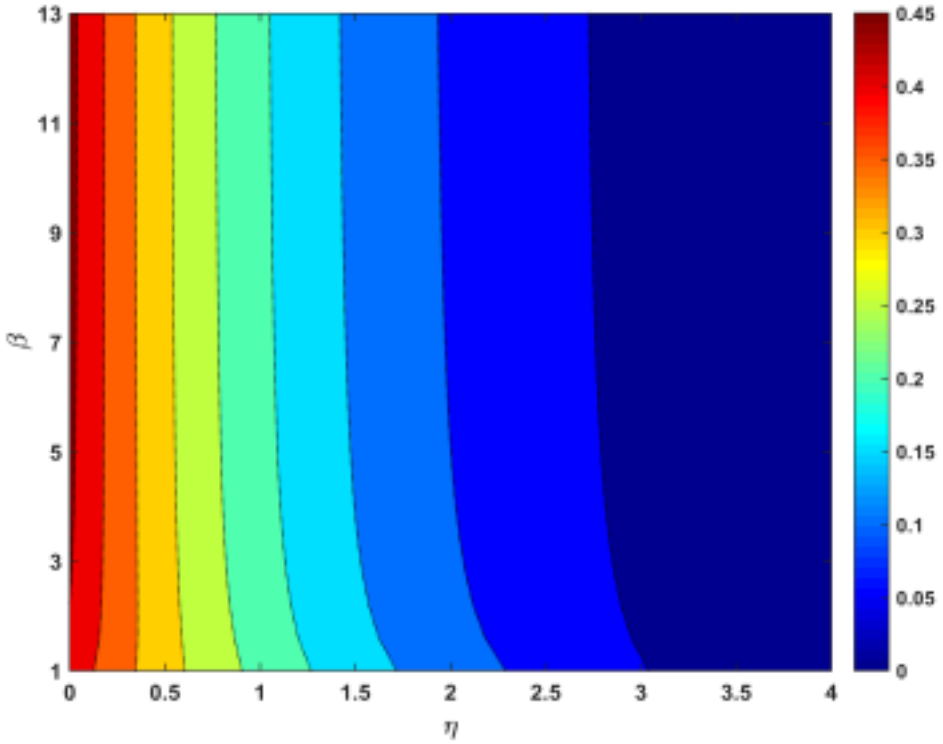

Figure 11.5: Deviations in $f'(\eta)$ with β

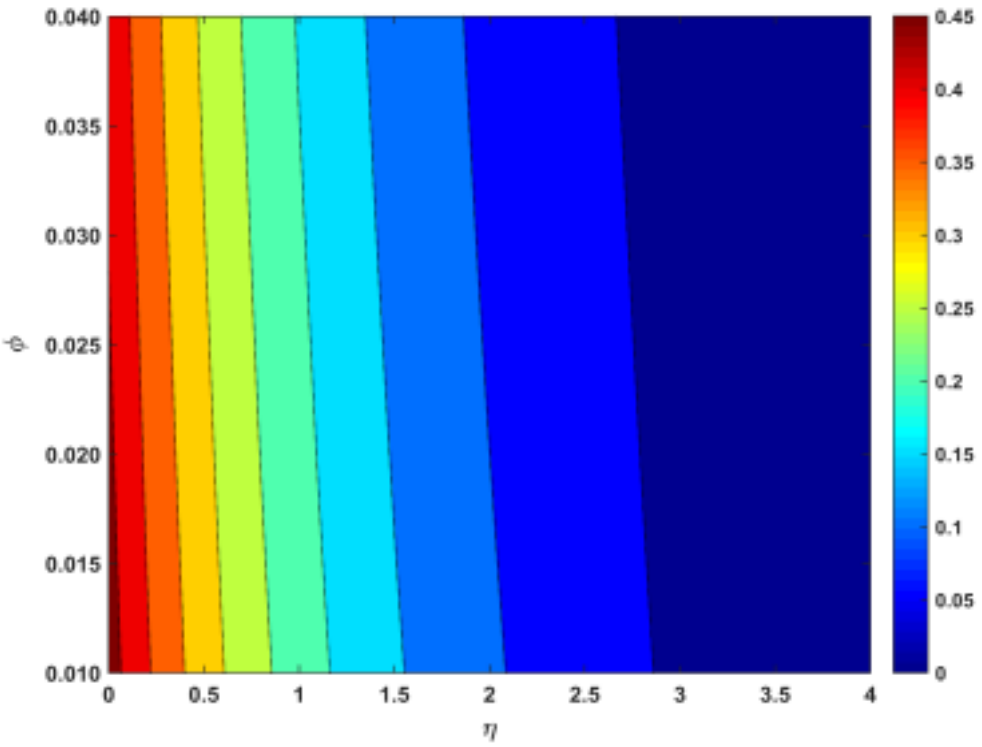

Figure 11.6: Deviations in $f'(\eta)$ with ϕ

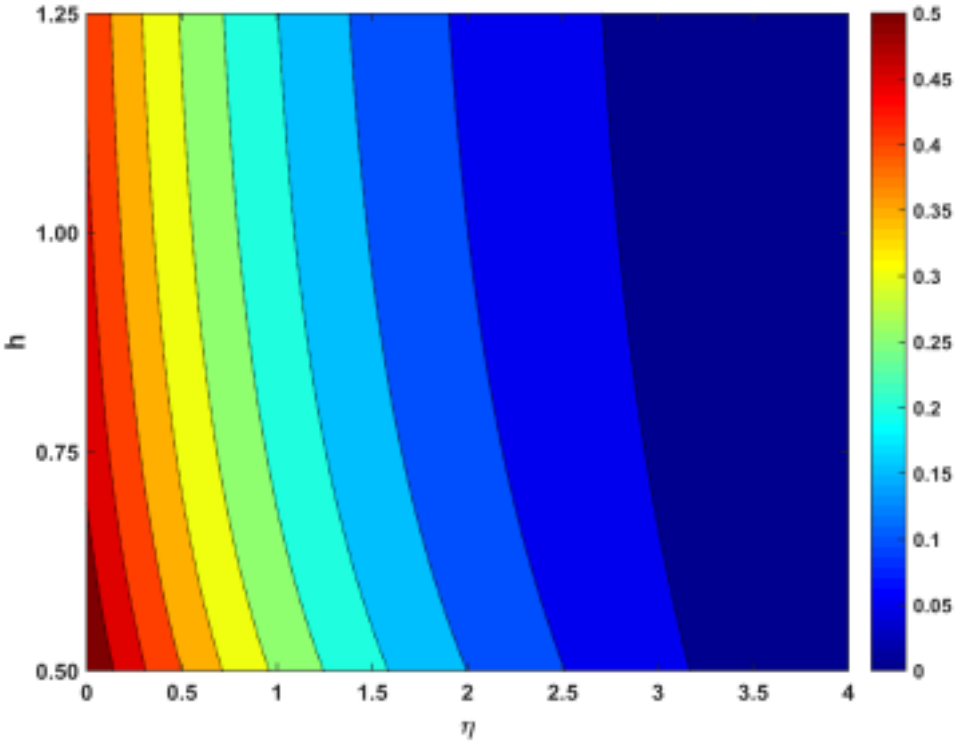

Figure 11.7: Deviations in $f'(\eta)$ with h

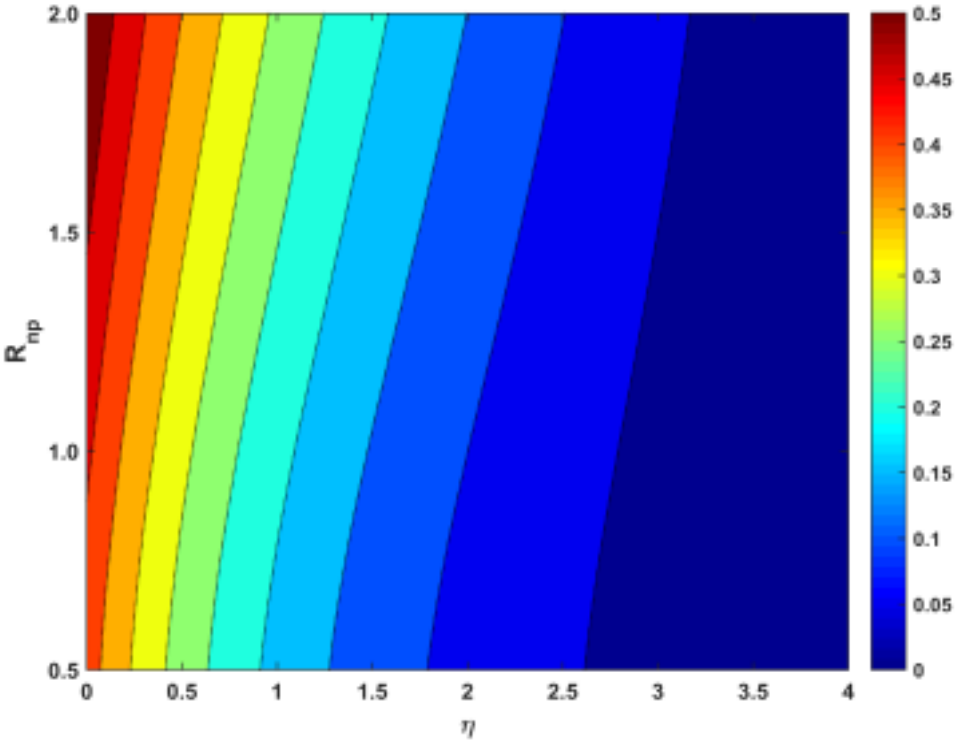

Figure 11.8: Deviations in $f'(\eta)$ with R_{np}

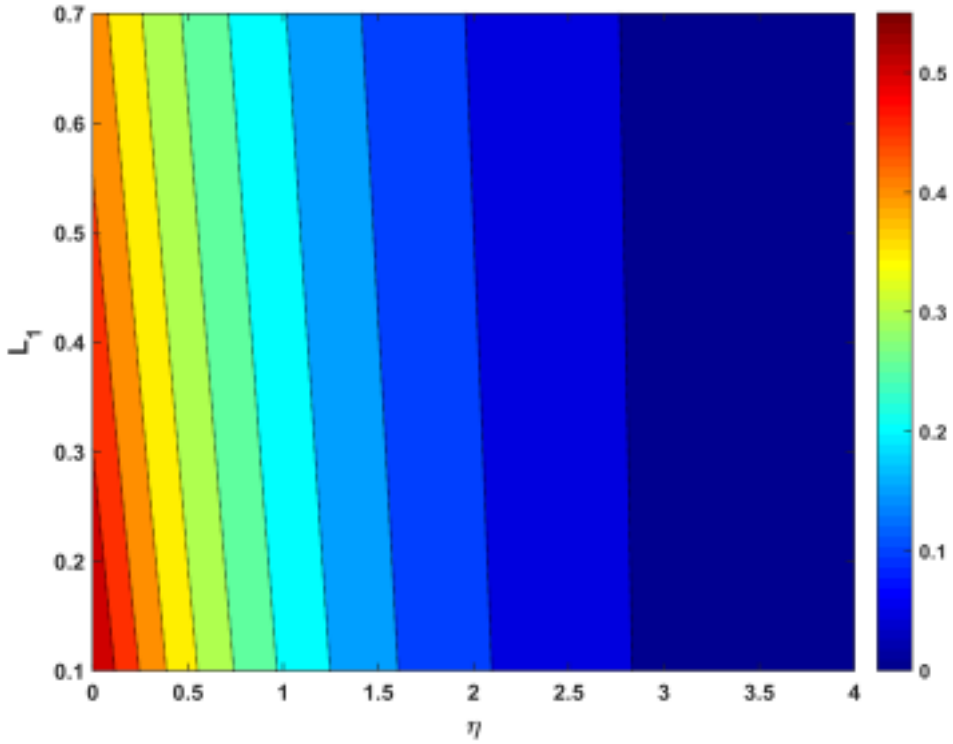

Figure 11.9: Deviations in $f'(\eta)$ with L_1

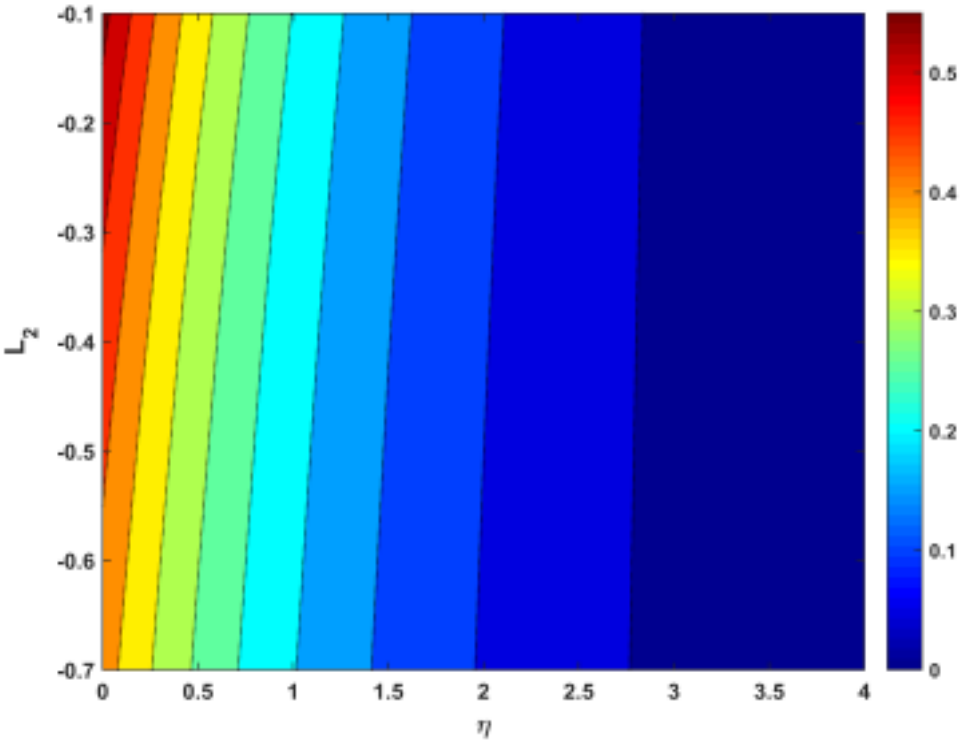

Figure 11.10: Deviations in $f'(\eta)$ with L_2

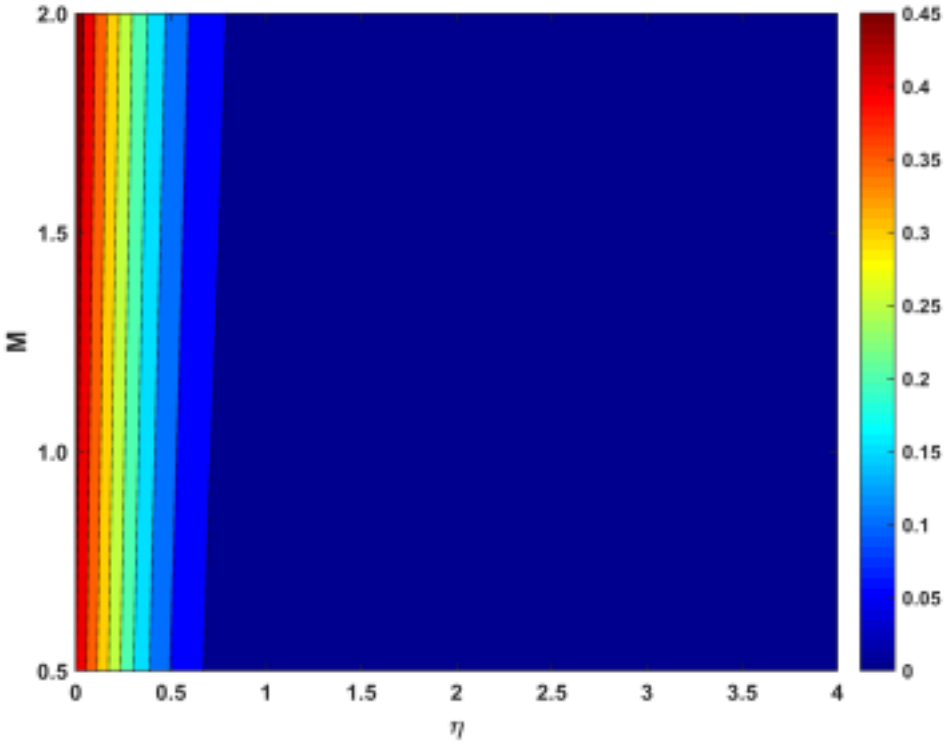

Figure 11.11: Deviations in $\theta(\eta)$ with M

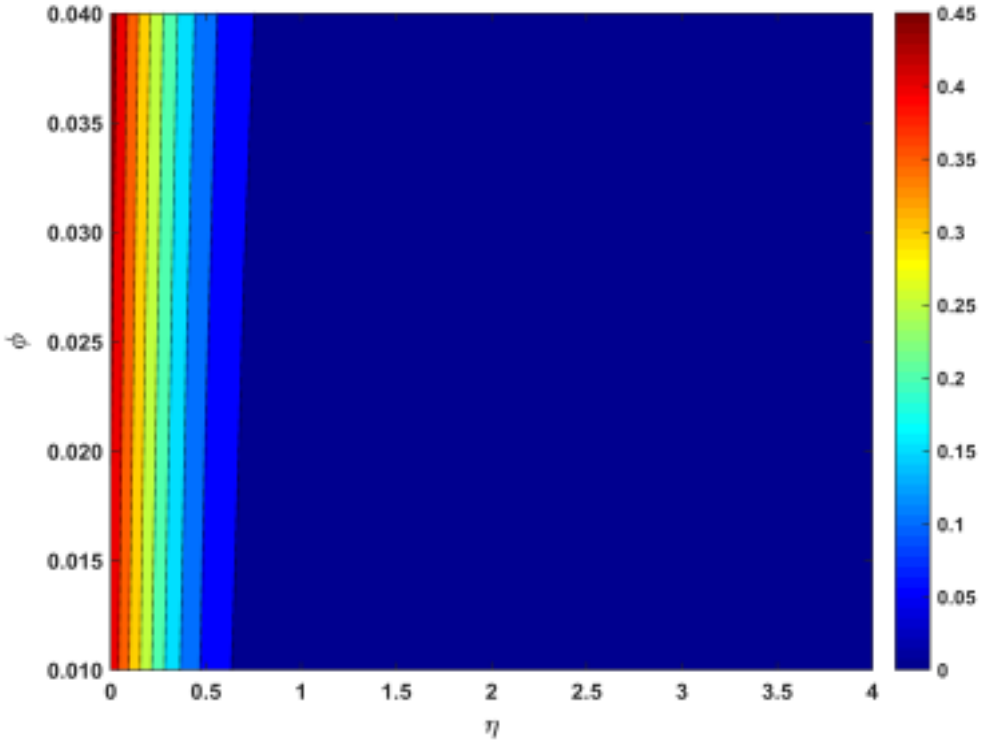

Figure 11.12: Deviations in $\theta(\eta)$ with ϕ

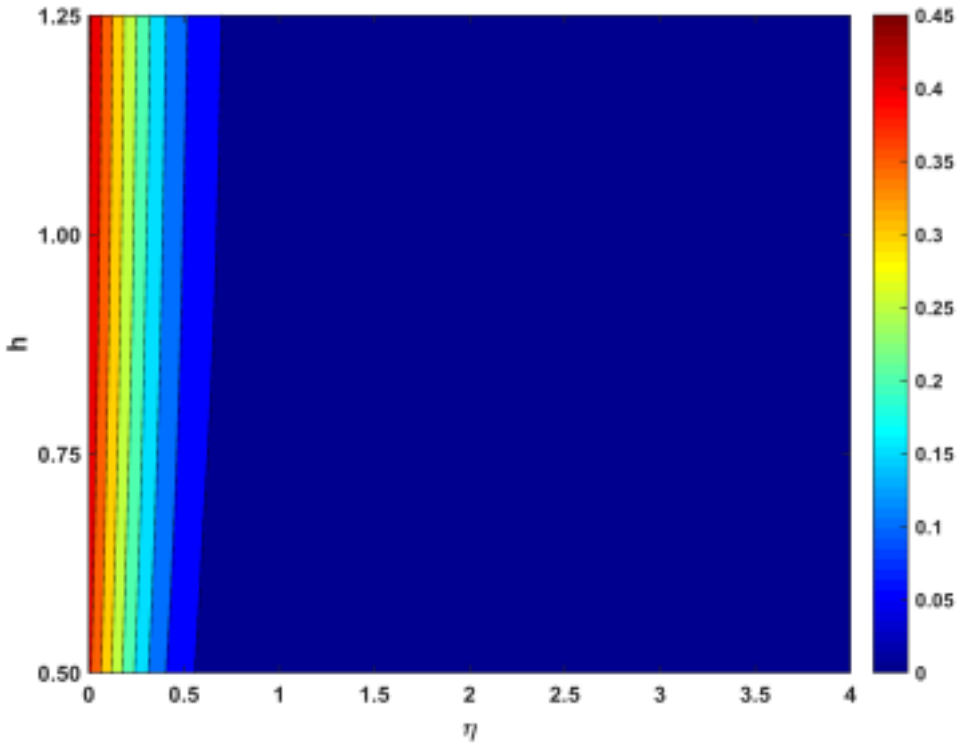

Figure 11.13: Deviations in $\theta(\eta)$ with h

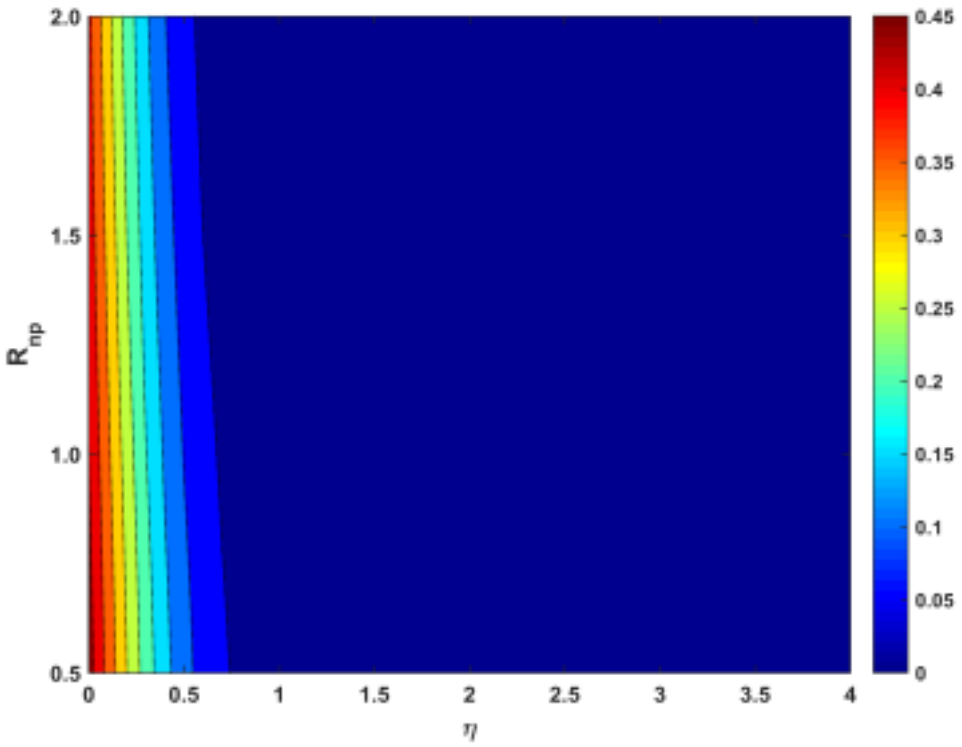

Figure 11.14: Deviations in $\theta(\eta)$ with R_{np}

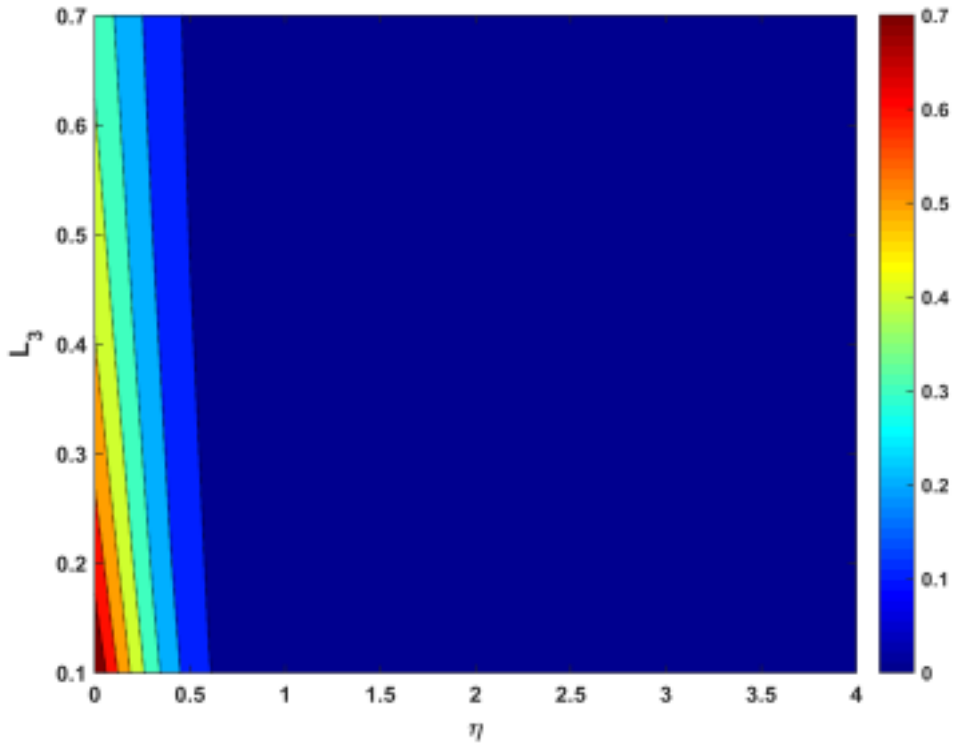

Figure 11.15: Deviations in $\theta(\eta)$ with L_3

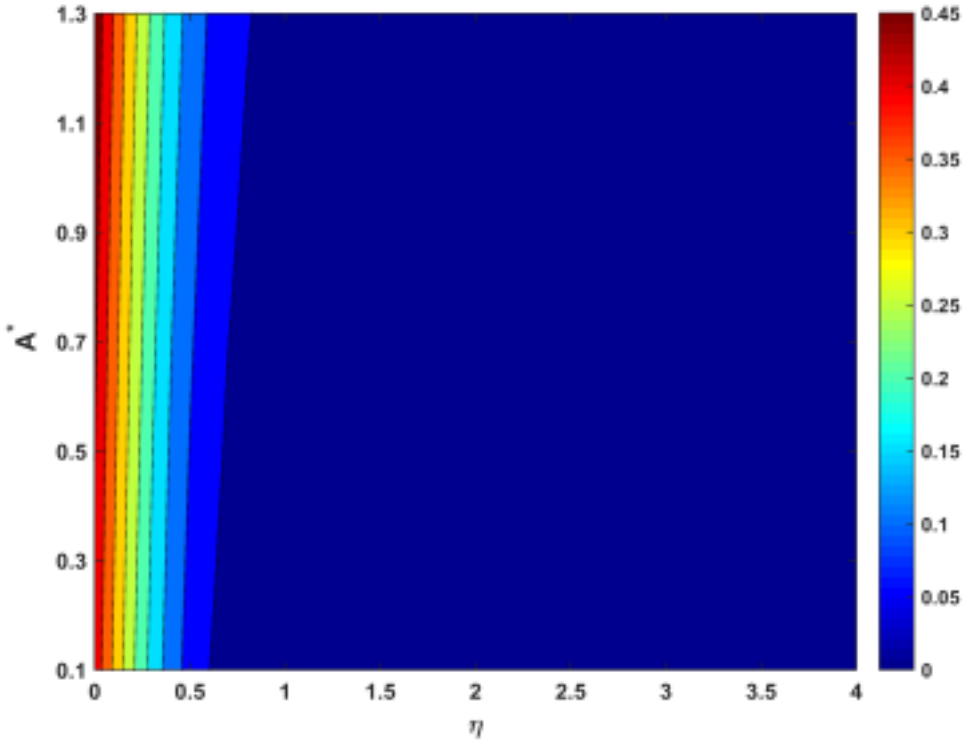

Figure 11.16: Deviations in $\theta(\eta)$ with A^*

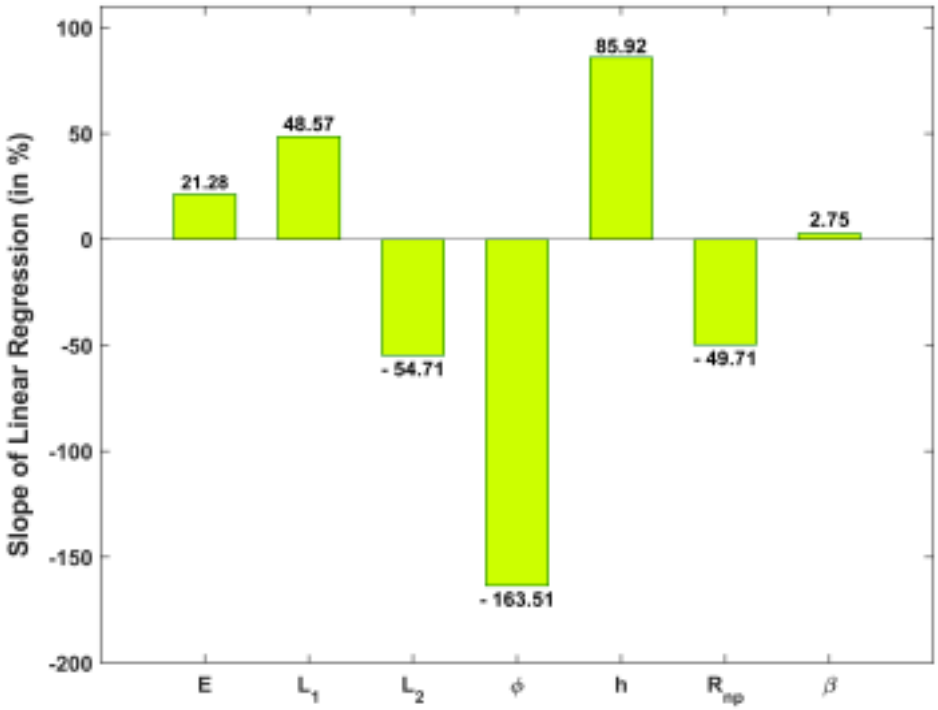

Figure 11.17: Deviations in $Cf_x Re_x^{1/2}$ with differing parameters

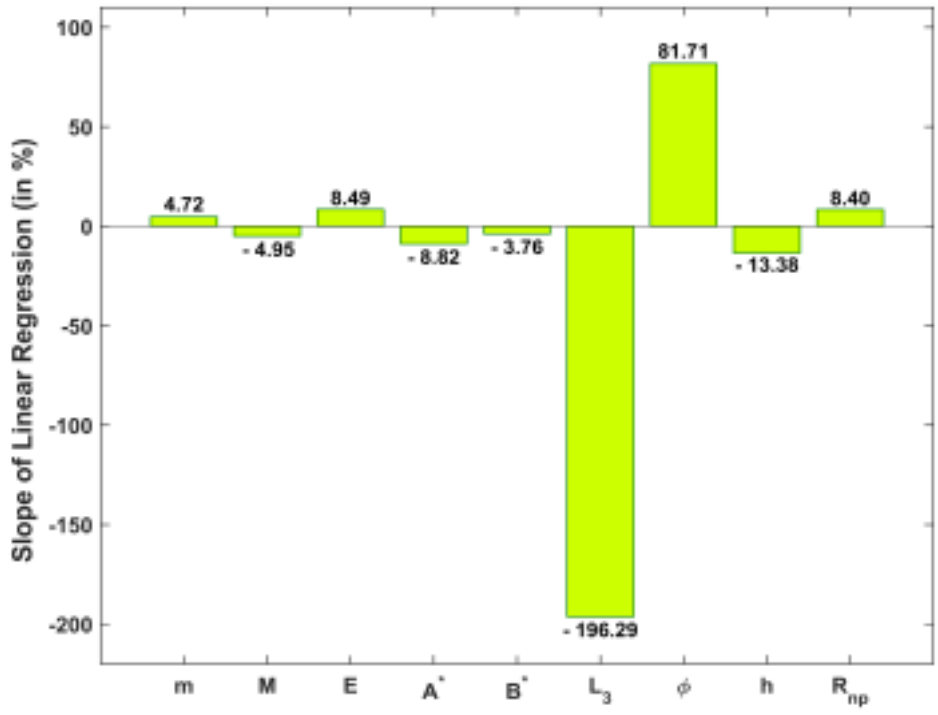

Figure 11.18: Deviations in $Nu_x Re_x^{-1/2}$ with differing parameters

The generation of Lorentz force with the supply of M tends to increase $\theta(\eta)$ (see Figure 11.11). The addition of gold-nanoparticles alters the thermophysical properties that in-turn increases the thermal field (see Figure 11.12). The constructive of inter-particle spacing of gold-nanoparticles on $\theta(\eta)$ has been elucidated through Figure 11.13. Figure 11.14 depicts the destructive effect of the radius of gold-nanoparticle on $\theta(\eta)$. From Figure 11.15, it is evident that the change in 1st order thermal slip parameter is inversely proportional to the thermal field. The augmentation of SHS parameter values induces a supplement energy that increases the temperature profile (see Figure 11.16).

Figures 11.17 - 11.18 graphically represent the trend and magnitude of the change in the drag rate and heat transfer rate with respect to effectual parameters. The following are inferred from Figures 11.17 - 11.18:

- Per unit increase in E augments $Cf_x Re_x^{1/2}$ and $Nu_x Re_x^{-1/2}$ by 21.28% and 8.49%, respectively.

- Per unit increase in the volume fraction of gold nanoparticles augments the $Nu_x Re_x^{-1/2}$ by 81.71% and reduces $Cf_x Re_x^{1/2}$ by 163.51%. Physically, this is due to the improved thermophysical properties of the nanofluid.

- Per unit increase in the inter-particle spacing of gold nanoparticles augments $Cf_x Re_x^{1/2}$ by 85.92% and decreases $Nu_x Re_x^{-1/2}$ by 13.38%.

- Per unit increase in the radius of gold nanoparticles augments $Nu_x Re_x^{-1/2}$ by 8.40% and reduces $Cf_x Re_x^{1/2}$ by 49.71%. Physically, an increase in nanoparticle radius implies an increase in the net amount of nanoparticle in the nanofluid mixture that results in the improvement of nanofluid's thermophysical properties.

- Per unit increase in the 1st order velocity-slip parameter augments the drag coefficient by 48.57% whereas the 2nd order velocity-slip parameter decreases the surface drag by 54.71%.

- Per unit increase in the thermal-slip parameter reduces the heat transfer rate by 196.29%.

- $Nu_x Re_x^{-1/2}$ is maximum for smaller values of $M,\ A^*,\ B^*,\ L_3,\ h$ and larger values of $m,\ E,\ \phi,\ R_{np}$.

- $Cf_x Re_x^{1/2}$ is minimum for smaller values of $E,\ L_1,\ h,\ \beta$ and larger values of $L_2,\ \phi,\ R_{np}$.

11.5 Conclusion

The significance of 2nd order velocity slip, nanoparticle radius, 1st order thermal slip and non-uniform heat source on the electro-magnetohydrodynamic blood-gold Casson nanofluid flow over a nonlinearly stretched surface has been numerically elucidated. The present study finds its application in radiofrequency ablation, magnetic resonance imaging, cancer therapy, and targeted drug delivery. The major findings of the study are:

- The administration of an external electric-field ascends the velocity profile.

- The nanofluid velocity is observed to descend with an increase in the Casson parameter.

- The addition of gold-nanoparticles and an increase in the inter-particle spacing of gold-nanoparticles descends the velocity profile. However, a reverse trend is observed when the radius of gold-nanoparticles is augmented.

- The 2nd order hydrodynamic-slip parameter ascends the nanofluid velocity whereas the 1st order hydrodynamic-slip parameter descends the velocity profile.

- The lowest surface drag is noted for smaller values of Casson parameter.

- The addition of gold-nanoparticles and an increase in the inter-particle spacing of gold-nanoparticles ascends the thermal field. However, a reverse trend is observed when the radius of gold-nanoparticles is augmented.

- The highest heat transfer rate is noticed for lower values of SHS and THS parameters.

- Per unit increase in the electric-field parameter augments the drag coefficient and heat transfer rate by 21.28% and 8.49%, respectively.

- Per unit increase in the volume fraction of gold nanoparticles augments the heat transfer rate by 81.71% and reduces the surface drag by 163.51%.
- Per unit increase in the inter-particle spacing of gold nanoparticles augments the drag coefficient by 85.92% and decreases the heat transfer rate by 13.38%.
- Per unit increase in the radius of gold nanoparticles augments the heat transfer rate by 8.40% and reduces the surface drag by 49.71%.
- Per unit increase in the 1st order velocity-slip parameter augments the drag coefficient by 48.57% whereas the 2nd order velocity-slip parameter decreases the surface drag by 54.71%.

Appendix I: Non-dimensional qunatities

$E = \dfrac{E_0}{B_0\ u_w}$	Electric-field parameter
$L_1 = N_1 \sqrt{\dfrac{a}{\vartheta_f}}$	1st order velocity-slip parameter
$L_2 = N_2\ \dfrac{a}{\vartheta_f}$	2nd order velocity-slip parameter
$L_3 = N_3 \sqrt{\dfrac{a}{\vartheta_f}}$	1st order thermal-slip parameter
$M = \dfrac{\sigma_f\ {B_0}^2}{a\ \rho_f}$	Magnetic-field parameterr
$Pr = \dfrac{(\mu\ C_p)_f}{k_f}$	Prandtl numberr

Appendix II: Nomenclature

a	Positive constant	E_0	Strength of electric-field
u, v	Velocity components	B_0	Strength of magnetic field
q'''	Non-uniform heat source	T_∞	Ambient temperature
T	Fluid temperature	T_w	Wall temperature
x, y	Cartesian coordinates	u_w	Stretching velocity
τ_w	Wall shear stress	Nu_x	Local Nusselt number
ρC_p	Heat capacity	Cf_x	Local drag coefficient
σ	Electrical conductivity	μ	Dynamic viscosity
η	Similarity variable	ϑ	Kinematic viscosity
k	Thermal conductivity	β	Casson parameter
ρ	Density	ϕ	Nanoparticle volume fraction
R_{np}	Nanoparticle radius	N_1^*, N_2^*	Velocity-slip factors
N_3^*	Thermal-slip factor	m	Non-linear stretching parameter
h	Inter-particle spacing	A^*	Space-dependent heat source
q_w	Heat flux	B^*	Temperature-dependent heat source